Available online at www.sciencedirect.com
SCIENCE DIRECT®
International Journal of Heat and Fluid Flow 24 (2003) 888–901
International Journal of HEAT AND FLUID FLOW
www.elsevier.com/locate/ijhff

Convection regimes and heat transfer characteristics along a continuously moving heated vertical plate

Sami A. Al-Sanea *

Department of Mechanical Engineering, College of Engineering, King Saud University, P.O. Box 800, Riyadh 11421, Saudi Arabia

Received 9 July 2002; accepted 11 January 2003

Abstract

The steady laminar flow and thermal characteristics of a continuously moving vertical sheet of extruded material are studied close to and far downstream from the extrusion slot. The velocity and temperature variations, obtained by a finite volume method, are used to map out the entire forced, mixed and natural convection regimes. The effects of the Prandtl number (Pr) and the buoyancy force parameter (B) on the friction and heat transfer coefficients are investigated. Comparisons with experimental measurements and solutions by others in the pure forced and pure natural convection regions are made. In the mixed convection region, the results are compared with available finite-difference solutions of the boundary layer equations showing excellent agreement. The region close to the extrusion slot is characterized as a non-similar forced-convection dominated region in which $Nu_x Re_x^{-1/2}$ drops sharply with increasing Richardson number (Ri_x). This is followed by a self-similar forced-convection dominated region in which $Nu_x Re_x^{-1/2}$ levels off with increasing Ri_x until the buoyancy effect sets in. The existence and extent of the latter region depend upon the value of B. A non-similar mixed convection region where increasing buoyancy effect enhances the heat transfer rate follows. Finally, this region is followed downstream by a self-similar natural-convection dominated region in which $Nu_x Re_x^{-1/2}$ approaches the pure natural convection asymptote at large Ri_x. Critical values of Ri_x to distinguish the various convection regimes are determined for different Pr and B.

Keywords: Continuously moving surface; Mixed convection; Laminar convection regimes; Backward boundary layer

1. Introduction

A continuously moving surface through an otherwise quiescent fluid has many applications in manufacturing processes. Such processes are hot rolling, metal and plastic extrusion, continuous casting, glass fiber production, and paper production (Tadmor and Klein, 1970; Fisher, 1976; Altan et al., 1979). Knowledge of fluid flow and heat transfer is necessary for determining the quality of the final products of these processes (Karwe and Jaluria, 1988, 1991). This physical situation is different from that of the classical boundary-layer flow over a stationary flat plate (Blasius flow) because of fluid entrainment toward the moving surface. Sakiadis (1961a,b) was the first to recognize this backward boundary-layer situation and used a similarity transformation to obtain a numerical solution for the flow field of a continuously moving surface.

Since the pioneering work of Sakiadis, many authors have analyzed the hydrodynamic and thermal characteristics of such a class of boundary layer problems for various conditions. Tsou et al. (1967) reported, analytically and experimentally, the flow and thermal fields developed by a continuously moving surface and showed that this flow is physically realizable under laboratory conditions. Stretched surfaces with different velocity and temperature conditions at the surface were studied by Soundalgekar and Ramana Murty (1980), Grubka and Bobba (1985), Jeng et al. (1986) and Ali (1994).

The buoyancy force resulting from the temperature differences in the fluid can be important if the velocity of the moving surface is relatively low and the temperature difference between the surface and the fluid is large. This can affect significantly the velocity and temperature distributions and, hence, the heat transfer rate from the surface. Buoyancy effects in boundary layers on contin-

* Fax: +966-1-467-6652.
E-mail address: sanea@ksu.edu.sa (S.A. Al-Sanea).

0142-727X/$ - see front matter © 2003 Elsevier Inc. All rights reserved.
doi:10.1016/j.ijheatfluidflow.2003.10.001

Nomenclature

B	buoyancy force parameter $= Gr_x/Re_x^3 = g\beta(T_w - T_\infty)v/u_w^3$
$C_{f,x}$	local skin-friction coefficient $= \tau_{w,x}/0.5\rho u_w^2$
$F_1(Pr)$	a function of Prandtl number $= 0.75Pr^{1/2}[2.5(1 + 2Pr^{1/2} + 2Pr)]^{-1/4}$
$F_2(Pr)$	a function of Prandtl number $= 1.886Pr^{13/32} - 1.445Pr^{1/3}$
Gr_x	local Grashof number $= g\beta(T_w - T_\infty)x^3/v^2$
h_x	local heat-transfer coefficient
k	thermal conductivity of fluid
L	domain length
Nu_x	local Nusselt number $= h_x x/k$
p	pressure
P	dimensionless pressure $= (p - p_\infty)/\rho u_w^2$
Pr	Prandtl number $= v/\alpha$
Re_x	local Reynolds number $= u_w x/v$
Ri_x	local Richardson number $= Gr_x/Re_x^2 = g\beta(T_w - T_\infty)x/u_w^2$
S	source term
T	temperature
u	velocity component in x-direction
u_w	surface velocity
U	dimensionless velocity component $= u/u_w$
U^*	dimensionless velocity component $= uxGr_x^{-1/2}/(2v)$
v	velocity component in y-direction
V	dimensionless velocity component $= v/u_w$
x	coordinate along direction of surface motion
X	dimensionless coordinate $= x/L$
y	coordinate along direction normal to surface motion
Y	dimensionless coordinate $= y/L$

Greeks

α	thermal diffusivity
β	volumetric thermal expansion coefficient
Γ	dimensionless exchange coefficient
η_1	dimensionless similarity variable $= (y/x)Re_x^{1/2}$
η_2	dimensionless similarity variable $= (y/x)(Gr_x/4)^{1/4}$
θ	dimensionless temperature $= (T - T_\infty)/(T_w - T_\infty)$
v	kinematic viscosity
ρ	density
$\tau_{w,x}$	local shear stress
ϕ	a general dependent variable

Subscripts

c	critical conditions
e	pertains to entrained velocity
w	condition at surface
ϕ	a general dependent variable
∞	condition at ambient medium

uously moving surfaces through an otherwise quiescent fluid have been studied by Chen and Strobel (1980) and Fan et al. (1997) for horizontal surfaces, by Chen (1998), Ali and Al-Yousef (1998) and Fan et al. (1999) for vertical surfaces, and by Moutsoglou and Chen (1980), Strobel and Chen (1980) and Chen (2000) for vertical and inclined surfaces. In the presence of buoyancy forces, similarity solutions do not exist except for a restricted power-law surface velocity and temperature distributions.

Mixed convection correlations for continuous moving sheets were reviewed by Chen and Armaly (1987). They reported extensive correlations for horizontal, inclined and vertical moving sheets and for both the uniform wall temperature and uniform heat flux boundary conditions in buoyancy-assisting and buoyancy-opposing situations. In a more recent review, Viskanta and Bergman (1998) discussed several aspects related to the moving plate problem. These include, for example, the effects of the conjugate boundary conditions at the plate surface, the effects of an externally induced forced flow (moving plate in a parallel channel flow) and the effects of suction and injection through a stretched surface.

In almost all the papers cited earlier, the studies concentrated on the boundary layer far away from the extrusion slot where the boundary layer approximations are valid. However, the flow and heat transfer characteristics are also important close to the slot where both the friction and heat transfer coefficients attain their largest values. A more general finite-difference formulation using the full elliptic governing equations including buoyancy effects was employed by Karwe and Jaluria (1988, 1991) and Kang and Jaluria (1994). The effect of buoyancy was found to be more prominent when the plate moves vertically upward than when it moves horizontally. It was also found that the elliptic effects are important near the extrusion slot and decay downstream. In a recent study, Al-Sanea and Ali (2000) investigated the effects of the extrusion die and of suction and injection at the moving surface on the friction and heat-transfer coefficient distributions with emphasis on the region close to the extrusion slot using the full elliptic equations. Critical Reynolds numbers to distinguish between the self-similar and non-similar regions were also determined. However, the buoyancy effects were not accounted for and, hence, only the pure forced convection regime was analyzed.

The present investigation examines the effect of buoyancy on the flow and thermal characteristics close to and far downstream from the extrusion slot for different Prandtl number fluids and buoyancy force

parameter values. Another objective is to determine the critical values of Richardson number to delineate the forced, mixed and natural convection regimes for a continuously moving vertical heated surface.

2. Mathematical formulation and calculation procedure

2.1. Basic assumptions and governing equations

Fig. 1 shows a continuously moving vertical heated plate emerging from a slot at a velocity u_w and a temperature T_w in an otherwise quiescent fluid. The gravitational body force is oriented in the negative x-direction. The induced motion of the fluid is assumed to be laminar, steady, and two-dimensional with thermally active incompressible viscous fluid with constant properties. Further simplification is made through the use of the Boussinesq approximation. Subject to these assumptions, the full elliptic governing equations can be written as

$$\frac{\partial U}{\partial X}+\frac{\partial V}{\partial Y}=0 \tag{1}$$

$$\frac{\partial}{\partial X}(U^2)+\frac{\partial}{\partial Y}(UV)-\frac{1}{Re_{\mathrm{L}}}\left(\frac{\partial^2 U}{\partial X^2}+\frac{\partial^2 U}{\partial Y^2}\right)=-\frac{\partial P}{\partial X}+\frac{Gr_{\mathrm{L}}}{Re_{\mathrm{L}}^2}\theta \tag{2}$$

$$\frac{\partial}{\partial X}(UV)+\frac{\partial}{\partial Y}(V^2)-\frac{1}{Re_{\mathrm{L}}}\left(\frac{\partial^2 V}{\partial X^2}+\frac{\partial^2 V}{\partial Y^2}\right)=-\frac{\partial P}{\partial Y} \tag{3}$$

$$\frac{\partial}{\partial X}(U\Theta)+\frac{\partial}{\partial Y}(V\Theta)-\frac{1}{Re_{\mathrm{L}}Pr}\left(\frac{\partial^2 \Theta}{\partial X^2}+\frac{\partial^2 \Theta}{\partial Y^2}\right)=0 \tag{4}$$

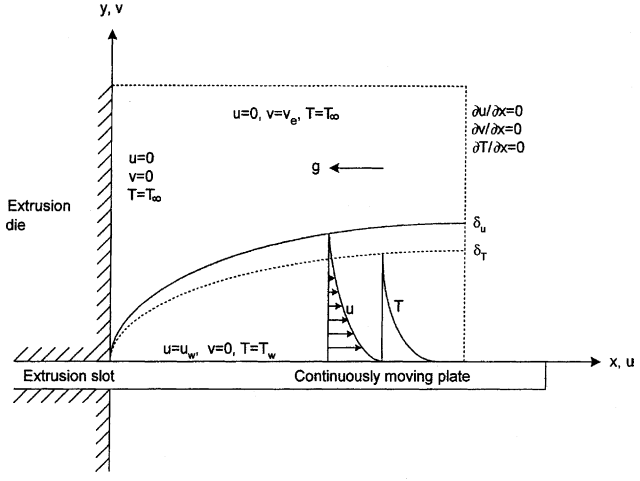

Fig. 1. A schematic showing the physical situation and boundary conditions of a continuously moving plate.

The length, velocity, temperature and pressure scales selected to normalize the equations are L, u_w, $(T_w - T_\infty)$ and ρu_w^2, respectively. The above set of equations can be represented by a single equation of the form:

$$\frac{\partial}{\partial X}(U\phi)+\frac{\partial}{\partial Y}(V\phi)-\frac{\Gamma_\phi}{Re_{\mathrm{L}}}\left(\frac{\partial^2\phi}{\partial X^2}+\frac{\partial^2\phi}{\partial Y^2}\right)=S_\phi \tag{5}$$

where ϕ is the general variable and stands for 1, U, V and Θ in Eqs. (1)–(4), respectively; Γ_ϕ is a dimensionless exchange coefficient whose values are 0, 1, 1 and $1/Pr$ in the above equations, respectively; and S_ϕ is a source term that represents the right-hand-side of the equations. This general form of transport equation facilitates the use of the same solution procedure for all equations.

2.2. Boundary conditions

With reference to Fig. 1, where the continuously moving plate is drawn vertically upward from the slot at $x = 0$ through an otherwise quiescent fluid, the following boundary conditions are applied. Starting with conditions at the plate surface ($y = 0$):

$$u=u_w,\quad v=0,\quad \text{and}\quad T=T_w \tag{6}$$

where u_w and T_w are constants.

The surface of the extrusion die, with the exception of the slot, represents an impervious and stationary wall at which:

$$u=0,\quad v=0,\quad \text{and}\quad T=T_\infty \tag{7}$$

It was found in a previous study that this side wall has an effect in creating a flow re-circulation region outside the boundary layer as a result of fluid entrainment toward the moving plate (Al-Sanea and Ali, 2000). Therefore, the region close to the extrusion slot is strictly elliptic and the boundary layer approximations cannot be applied.

The free stream boundary is located far away from the moving plate, therefore:

$$u=0,\quad v=v_e,\quad T=T_\infty,\quad \text{and}\quad p=p_\infty \tag{8}$$

This boundary is allowed to entrain fluid at velocity v_e and temperature T_∞. The velocity v_e is not known beforehand and is determined iteratively by the calculations. Its value depends upon the mass flow rate drawn outside the calculation domain by the viscous action of the moving plate.

The following conditions are applied at the outlet boundary:

$$\frac{\partial u}{\partial x}=0,\quad \frac{\partial v}{\partial x}=0,\quad \frac{\partial T}{\partial x}=0\quad \text{and}\quad p=p_\infty \tag{9}$$

These approximate fully developed conditions and are quite adequate in the parabolic dominated flow region especially when the outlet is ensured to be located far downstream from the extrusion slot.

2.3. Numerical solution procedure

The numerical model uses a control-volume finite-difference method for discretizing the governing partial-differential equations, Eqs. (1)–(4), and is essentially the same as that used by Al-Sanea and Ali (2000). The pressure field and velocities are determined via the well-known SIMPLE algorithm of Patankar and Spalding (1972), with a slight difference in the way the finite-volume equations are solved. The 2/E/FIX computer program of Pun and Spalding (1977) was modified and used to solve the present problem. The finite volume equations are handled by this code on a line-by-line manner. Al-Sanea et al. (1980) described and applied the line-by-line procedure in computing re-circulating flows with heat transfer. The scheme was found particularly beneficial for flows where relatively large parabolic or nearly parabolic regions exist along side the elliptic flow regions. The present moving plate problem falls into such a category where elliptic effects are dominant in the region close to the extrusion slot while far enough downstream the flow is predominantly parabolic.

All the numerical results are checked to be substantially grid independent. This is achieved by obtaining solutions with an increasing number of grid nodes until a stage is reached where the solution exhibits negligible change with further increase in the number of nodes. The boundary layer thickness increases with distance downstream from the slot and its thickness depends on the values of Reynolds number, Prandtl number and the buoyancy force parameter. Therefore, the locations of the free stream and outlet boundaries are always checked by numerical experiments to be far enough not to influence the results in the region of interest. For example, the free stream boundary would be located at a distance of about 10% L which is greater than twice the maximum thickness of the boundary layer present at the very end of the plate for $Re_L = 10^4$, $Pr = 1$ and $B = 10^{-2}$.

A non-uniform finite-volume grid is used with nodes closely spaced in regions with steep variation of flow properties; namely, near to the extrusion slot and the plate. A grid size of 100×50 nodes in the x- and y-directions, respectively, is normally employed. The grid step sizes, Δx and Δy, increase in the x- and y-directions (see Fig. 1) with expansion factors of about 1.1 and 1.2, respectively.

Converged solutions are achieved when the changes in all variables, for all nodes, produced in successive iterations diminish and when the sums of the normalized absolute values of residual errors in the finite volume equations are reduced to a small value. Typical converged results are obtained after about 700 iterations starting from uniform initial fields; a near optimum relaxation factor in the range (0.2–0.5) is applied for the dependent variables. Considerably larger number of iterations is needed for the pure natural convection calculations and for those physical situations dominated by natural convection. The calculations require about 1.4×10^{-5} s of CPU time per iteration for each variable for each grid node on a Pentium 200 MMX microcomputer.

3. Results and discussion

The results cover the entire mixed convection regime, from pure forced convection to pure natural convection. Different Prandtl number fluids are investigated in the range $0.1 \leqslant Pr \leqslant 10$. Only buoyancy assisting flows are considered and a wide range of the buoyancy force parameter is covered, $10^{-6} \leqslant B \leqslant 1$. Particular emphasis is given to the region close to the extrusion slot where elliptic effects dominate. The various convection regimes are mapped for different Pr and B in terms of Re_x and Gr_x.

3.1. Numerical model validation

The numerical model is validated by comparing predictions with previously published results under forced, mixed and natural convection conditions. It is noted that experimental data on the moving plate problem, under the present conditions, are scarce and available mainly for the limiting case of forced convection.

3.1.1. Forced convection

The forced convection problem was studied in detail in both the non-similar and self-similar regions by Al-Sanea and Ali (2000), in which the numerical model was validated against the similarity method solutions and results by others. In the present study, further validation is carried out with emphasis on comparisons with measurements.

Fig. 2a shows a comparison between the present predictions and the velocity measurements of Tsou et al. (1967). The dimensionless velocity U is defined as u/u_w and η_1 is the similarity variable defined as $(y/x)Re_x^{1/2}$. The Reynolds number of the data ranges from 5×10^4 to 1.5×10^5. The similarity solution obtained by Tsou et al. is also shown on the figure as the dotted line and gives an excellent agreement with the present finite-volume results. Both solutions give very good agreement with the measurements. However, the data tend to fall slightly above the curves at large values of η_1; this was attributed to disturbances in the laboratory as was explained by Tsou et al. In the present calculations, self-similar velocity profiles are obtained for $Re_x > 1500$. The measurements were taken far enough downstream from the slot where the conditions were truly self-similar inside the boundary layer. Temperature measurements were not reported by Tsou et al. (1967) under laminar flow conditions.

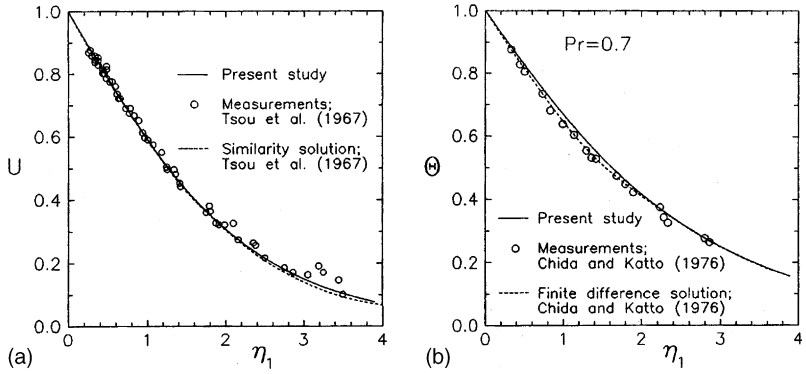

Fig. 2. Pure forced-convection dimensionless velocity and temperature distributions versus the similarity variable η_1 showing comparison with measurements and solutions by others at large Reynolds number; (a) velocity profile, and (b) temperature profile for $Pr = 0.7$.

Fig. 2b presents the dimensionless temperature distribution through the boundary layer formed on a continuously moving flat plate with constant surface temperature for $Pr = 0.7$. Comparisons with experimental measurements in air along with the finite difference solution of Chida and Katto (1976) show very good agreement. The Reynolds number of the experimental data ranges from 580 to 2100. In the present calculations, self-similar temperature profiles are obtained for $Re_x > 300$. It may be noted that achieving self-similarity for the velocity profiles is delayed further downstream compared to that for the temperature profiles due to the existence of reverse flow region outside the boundary layer and close to the extrusion slot which persists to $Re_x \approx 1000$ (Al-Sanea and Ali, 2000).

3.1.2. Mixed convection

Fig. 3a depicts Nusselt number variation with Richardson number showing comparisons between the present finite-volume elliptic solutions and the boundary layer solutions of Moutsoglou and Chen (1980) for different Prandtl numbers as presented by Chen and Armaly (1987). In order to absorb the effect of Pr and correlate the heat transfer results, Chen and Armaly replotted the results of Moutsoglou and Chen on a single graph with coordinates as shown in Fig. 3a. The Prandtl number functions $F_1(Pr)$ and $F_2(Pr)$ are defined in the nomenclature. The present results for $Pr = 0.7$ have also been presented for different values of the buoyancy force parameter (B). The results show that $Nu_x Re_x^{-1/2}$ increases with Ri_x far downstream from the extrusion slot. In the region close to the extrusion slot where the stream-wise diffusion becomes important, and hence the full Navier–Stokes equations need to be solved, the present predictions show a sharp increase in $Nu_x Re_x^{-1/2}$ with decreasing Ri_x. It is noted that the boundary layer solutions do not extend close to the extrusion slot. Besides, the present results show that the effect of B is confined to this elliptic region. More results and discussion regarding this point are given later. The agreement between the present predictions and those reported by Chen and Armaly (1987) is excellent.

The corresponding results for the local skin-friction coefficient variation with dimensionless distance along the plate are presented for different values of B in Fig. 3b in terms of $C_{f,x} Re_x^{1/2}$ versus Ri_x. The results are compared with those obtained by Moutsoglou and Chen (1980) using the boundary layer approximations for

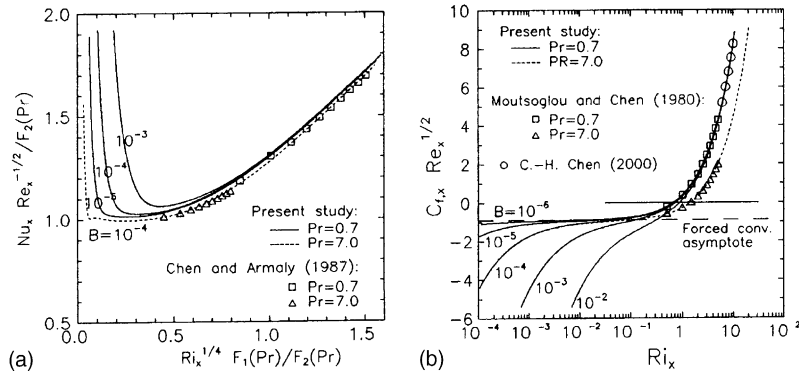

Fig. 3. Mixed convection Nusselt number and skin-friction coefficient variations with Richardson number showing comparison with boundary layer solutions; (a) Nusselt number, and (b) skin-friction coefficient.

$Pr = 0.7$ and 7, and those of Chen (2000) for $Pr = 0.7$. The shear stress at the wall is negative when the surface velocity is greater than the adjacent fluid velocity. The positive shear stress indicates the opposite due to velocity overshoot caused by buoyancy effect at large Ri_x. The zero shear stress does not imply boundary layer separation but corresponds to equal surface and adjacent fluid velocities. Once again, the results for different B collapse onto one line as Ri_x increases. At low Ri_x, the effect of B is clear, and as B is reduced the results approach the forced convection asymptote. The pure forced convection value of $C_{f,x}Re_x^{1/2}$, as calculated from the present results, is −0.8873 which agrees very well with −0.8875 found by Moutsoglou and Chen. Also, the agreement between the present results in the mixed convection region and those by Moutsoglou and Chen, and Chen is excellent. The zero shear stress for $B = 10^{-4}$ are calculated at $Ri_x = 0.673$ and 1.425 for $Pr = 0.7$ and 7, respectively. The corresponding results of Moutsoglou and Chen using the boundary layer approximations are 0.676 and 1.430, respectively.

The departure of $C_{f,x}Re_x^{1/2}$ values from the forced convection asymptote as Ri_x increases is due to buoyancy forces which start to show an effect. It is noted that the results presented by Moutsoglou and Chen (1980) and Chen (2000) extend only to $Ri_x = 5$ and 10, respectively. As will be seen later, $Ri_x = 10$ falls short of the region where natural convection becomes dominant. On the other hand, the present results extend well into the pure natural convection region.

3.1.3. Natural convection

The numerical model is also validated under pure natural convection conditions. This is affected by setting $u_w = 0$ in which the inertia forces vanish and the flow would be driven by buoyancy forces only. Under these conditions, the local Nusselt number is a function of Pr and Gr_x. Fig. 4a depicts the variation of $Nu_x Gr_x^{-1/4}$ with Gr_x for different Pr. At large values of Gr_x, $Nu_x Gr_x^{-1/4}$ is a function of Pr only. This is true in the self-similar region where the stream-wise diffusion is very small and can be neglected and, therefore, the boundary layer approximations are valid. However, at small values of Gr_x, $Nu_x Gr_x^{-1/4}$ is not a constant for a given Pr and increases rather sharply with decreasing Gr_x as shown in the figure. At low enough Gr_x, viscous forces dominate over the buoyancy forces and the energy equation reduces to a pure conduction equation in which Pr has no relevance. The results in Fig. 4a show this behavior clearly in which $Nu_x Gr_x^{-1/4}$ becomes independent of Prandtl number and, for the Prandtl number range investigated in the present study, all results collapse onto a single line for $Gr_x < 10^{-1}$. At the other extreme of large Gr_x, $Nu_x Gr_x^{-1/4}$ reach asymptotically the self-similar values for each value of Prandtl number as indicated by the long-dashed horizontal straight lines. These self-similar asymptotic values, as reported in Kays and Crawford (1993), agree extremely well with the present finite-volume results as shown in Fig. 4b.

The short dashed line drawn in Fig. 4a distinguishes the self-similar natural convection region to the right (region II) from the non-similar natural convection region to the left (region I) by connecting the critical values of Grashof numbers ($Gr_{x,c}$) for different values of Pr. These critical values are calculated by applying the "5% criterion", i.e. a $Gr_{x,c}$ value is obtained for a given Pr by calculating Gr_x at which $Nu_x Gr_x^{-1/4}$ deviates by 5% from its asymptotic self-similar value. The results show that $Gr_{x,c}$ decreases as Pr increases.

3.2. Velocity and temperature distributions

Representative dimensionless velocity profiles at different stream-wise locations given by Ri_x are displayed in Fig. 5a–d for $Pr = 1$ and $B = 10^{-2}$. In Fig. 5a and b, the u-velocity component normalized by the moving plate velocity ($U = u/u_w$) is plotted versus the transverse distance y normalized by the plate length ($Y = y/L$). Fig. 5a covers the region close to the extrusion slot where forced convection dominates, while Fig. 5b (note

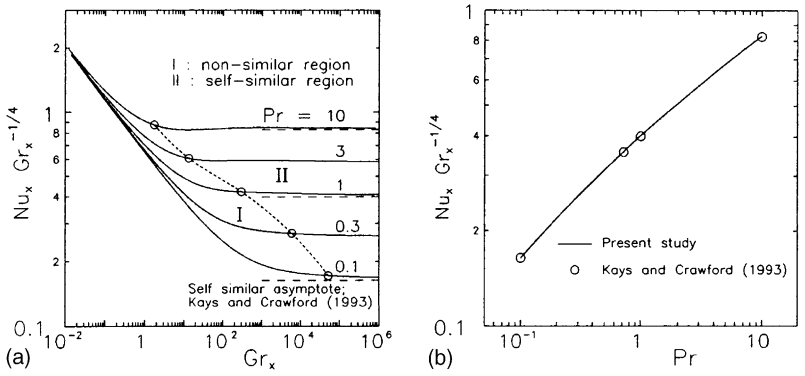

Fig. 4. Pure natural-convection heat transfer results showing comparison with asymptotic values for different Pr; (a) Nusselt number variation with Grashof number, and (b) Nusselt number variation with Prandtl number at large Gr_x.

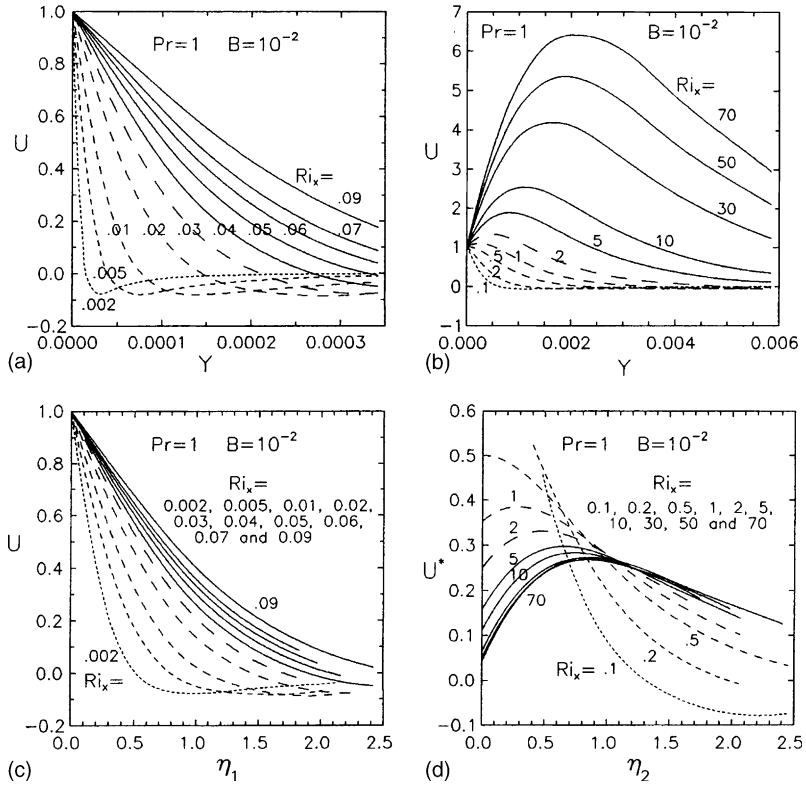

Fig. 5. Dimensionless velocity distributions for different Richardson numbers, $Pr = 1$ and $B = 10^{-2}$; (a) and (b) versus the transverse coordinate Y, and (c) and (d) versus the similarity variables η_1 and η_2.

the change in scale) extends over the entire mixed convection region and well into the natural convection region (these regions will be delineated clearly later).

Fig. 5a shows negative velocities outside the boundary layer and close to the extrusion slot (low Ri_x). This indicates the presence of reverse flow as a consequence of an adverse pressure gradient directed toward the slot. The latter is created by the action of the moving plate, fluid entrainment toward the plate surface and the effect of the side wall (extrusion die). This re-circulation region disappears further downstream with increasing Ri_x. The stream-wise velocity approaches the stagnant ambient value as Y increases; also, the velocity gradient at the plate $(Y = 0)$ decreases with increasing Ri_x as the boundary layer thickens. It is noted that the velocity profile starts to bulge upward for $Ri_x > 0.5$, see Fig. 5b, and there is a velocity overshoot for $Ri_x > 1$ due to the action of buoyancy which increases with Ri_x. At $Ri_x = 70$, the maximum velocity in the boundary layer is over six times that of the moving plate. The maximum velocity location shifts away from the plate surface with increasing Ri_x. It is also interesting to note that the velocity gradient at the surface changes sign at Ri_x between 0.5 and 1 where the absolute value of shear stress decreases to zero and then increases further downstream. This behavior can be realized by reference to Fig. 3b where the zero shear stress is calculated at $Ri_x = 0.878$ for $Pr = 0.7$ and $B = 10^{-2}$.

The same velocity distributions in Fig. 5a and b are re-plotted in Fig. 5c and d versus η_1 and η_2; note that U^* replaces U. These parameters are defined as

$$\eta_1 = (y/x)Re_x^{1/2}$$
$$\eta_2 = (y/x)(Gr_x/4)^{1/4} \qquad (10)$$
$$U^* = uxGr_x^{-1/2}/(2v)$$

where η_1 and η_2 are the dimensionless similarity variables for the forced convection and natural convection, respectively, and U^* is the dimensionless u-velocity component more appropriate for use in natural convection. The velocity profiles in Fig. 5c for $0.03 < Ri_x < 0.09$ are closer to each other relative to the other profiles but are not close enough to be self similar. In such a forced-convection dominated region, self-similar velocity profiles would have been achieved at some distance further downstream (Al-Sanea and Ali (2000)). However, under the present conditions, mixed convection effects which manifest themselves at $Ri_x > 0.1$ (as will be seen later) do not allow similarity to take place. It is noted that similarity solutions are not attainable under the present mixed convection conditions. Much further downstream, and for $Ri_x > 30$, all velocity profiles collapse onto one self-similar dimensionless profile as shown in Fig. 5d. These similarity profiles fall in the natural convection dominated region. The maximum value of U^* in the self-similar pure nat-

ural-convection region is calculated to be 0.253 at $\eta_2 = 0.92$ which agree very well with the values of 0.254 and 0.88, respectively, as inferred from graphical representation in Schlichting (1979) for $Pr = 1$.

The corresponding results for the dimensionless temperature distribution are presented in Fig. 6a–d. Again, the profiles extend over a wide range of Ri_x starting from the forced-convection dominated region, covering the entire mixed convection region, and ending well into the self-similar natural-convection dominated region. It is clear that as Ri_x increases the thermal boundary layer thickness increases. Most interesting is that the temperature profiles collapse onto one self-similar profile for $0.02 < Ri_x < 0.09$, as indicated by the results in Fig. 6c, just before buoyancy starts to show an effect. Therefore, the temperature profiles attain self-similarity closer to the extrusion slot than the velocity profiles (cf. Fig. 5a). This is attributed to the presence of the flow re-circulation region (a non-uniform condition) just outside the velocity boundary layer. Incidentally, and for the same reason, the thickness of the thermal boundary layer is greater than that of the velocity boundary layer. Nearer to the extrusion slot, $Ri_x < 0.02$, the temperature profiles are non-similar. This distinguishes the forced convection non-similar region in which the boundary layer approximations break down. For $Ri_x > 0.09$, the temperature profiles versus η_1 start to deviate from the self-similar profile. This marks the start of the mixed convection region which precludes self similarity. As Ri_x increases to about 30, the temperature profiles collapse once again onto a single self-similar profile, but this time versus η_2 (Fig. 6d), as the buoyancy forces dominate over the inertia forces. Similarity solutions for pure natural convection are, therefore, attainable at $Ri_x > 30$ for $Pr = 1$.

Dimensionless temperature profiles for other values of Pr, which are not presented to conserve space, show that as Pr increases the thermal boundary layer thickness decreases, and as Ri_x increases, for a given Pr, the thermal boundary layer thickness increases as expected.

3.3. Heat transfer convection regimes

Fig. 7a and b present the heat transfer characteristics along the moving plate in terms of $Nu_x Re_x^{-1/2}$ versus Ri_x for $Pr = 1$ and different values of B. Fig. 7a shows an interesting feature for the individual behavior of each convection mode acting alone in the absence of the other mode. The solid lines are for both forced and natural convection acting together (mixed convection). It is emphasized that both B and Ri_x are not relevant to either of the pure forced convection or the pure natural

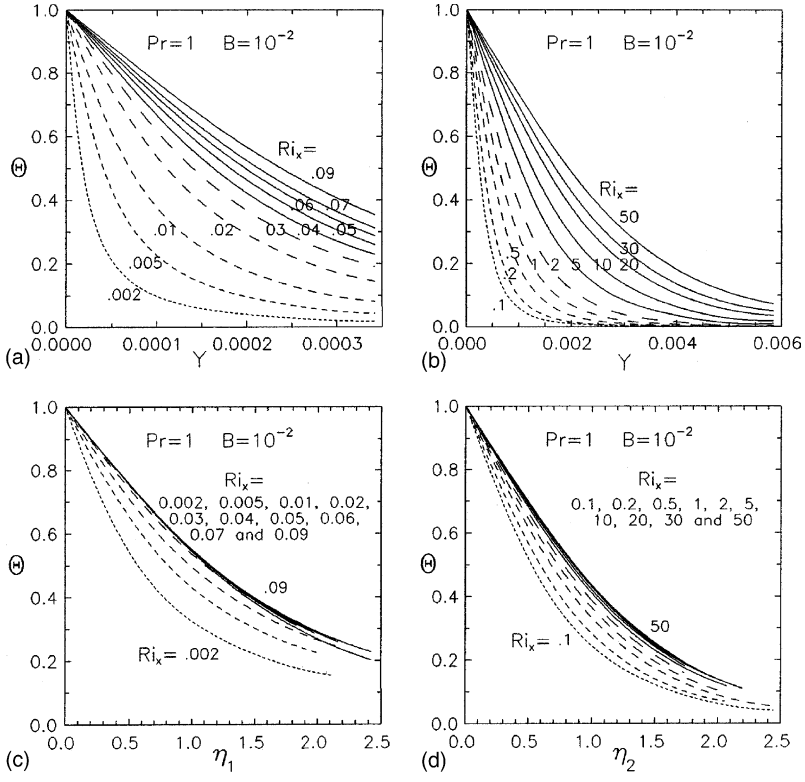

Fig. 6. Dimensionless temperature distributions for different Richardson numbers, $Pr = 1$ and $B = 10^{-2}$; (a) and (b) versus the transverse coordinate Y, and (c) and (d) versus the similarity variables η_1 and η_2.

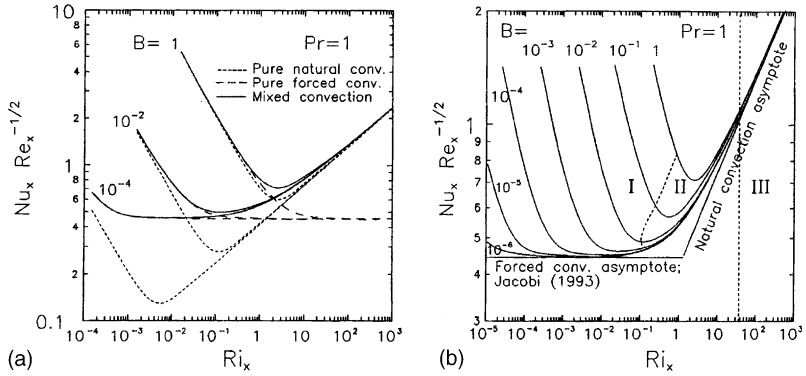

Fig. 7. Nusselt number variations with Richardson number for $Pr = 1$ and different B; (a) showing convection mode contribution, and (b) showing convection regimes.

convection; of course, Re_x and Gr_x are the appropriate dimensionless parameters for the forced and natural convection, respectively. However, the results are plotted versus Ri_x (a dimensionless distance along the surface) in order to have a direct comparison between the heat transfer results of the different convection modes and, also, to use a suitable criterion to delineate the forced, mixed and natural convection regimes. It is noted that the natural convection results in terms of $Nu_x Gr_x^{-1/4}$ have been transformed into the form of forced and mixed convection results in terms of $Nu_x Re_x^{-1/2}$ by using:

$$Nu_x Re_x^{-1/2} = Nu_x Gr_x^{-1/4} Ri_x^{1/4} \tag{11}$$

It should also be noted that the values of the parameter B in Fig. 7a have the mere effect of shifting the pure forced and natural convection results on the plot and appeared through the above transformation.

The pure forced convection results presented in Fig. 7a show that $Nu_x Re_x^{-1/2}$ decreases with increasing Ri_x and reaches a constant asymptotic value with a further increase in Ri_x. This constant value is the pure forced-convection asymptote in the self-similar forced convection region. A 5% increase in this value would mark the critical conditions that distinguish this region from the non-similar pure forced-convection region (Al-Sanea and Ali, 2000).

The pure natural convection results presented in Fig. 7a show that $Nu_x Re_x^{-1/2}$ decreases with increasing Ri_x to a minimum and then increases with Ri_x. The minimum value separates the natural convection non-similar region from the self-similar region. This has been discussed previously and presented in Fig. 4a for different Pr. The value of Nusselt number for pure natural convection becomes equal to that for pure forced convection around $Ri_x = 1$ at which there is an equal contribution to the heat transfer rate from either mode. For $Ri_x > 1$, the heat transfer rate due to pure natural convection becomes greater than that due to the pure forced convection.

It is interesting to note how $Nu_x Re_x^{-1/2}$ for mixed convection deviates (increases) gradually from the pure forced convection results with increasing Ri_x, for any value of B, and then approaches asymptotically the natural convection results at large Ri_x. The heat transfer results would also be independent of B at large Ri_x, since B is relevant only to mixed convection. An interesting behavior of the results in Fig. 7a is that $Nu_x Re_x^{-1/2}$ is the same for any convection mode at low Ri_x (depending upon B). This is due to the fact that at low Ri_x, the problem becomes dominated by diffusion and, hence, the temperature field and the heat transfer rate at the plate surface become independent of the velocity field and, therefore, independent of the heat convection mode. In practice, this region would occupy only a tiny part close to the extrusion slot.

A criterion used by previous investigators to delineate the mixed convection regime for the Blasius boundary-layer problem is used in the present study to delineate the convection regimes for the present moving plate problem. This is based on the "5% criterion", that is based on the heat transfer enhancement due to mixed convection over either of the pure forced or pure natural convection results. Therefore, a 5% increase in Nu_x over that of pure forced convection would mark the critical Richardson number ($Ri_{x,c1}$) that distinguishes the pure forced convection regime from the mixed convection regime. Similarly, a 5% increase in Nu_x over that of pure natural convection would mark $Ri_{x,c2}$ that distinguishes the pure natural convection regime from the mixed convection regime. This procedure is applied for different values of Pr and B (the parameters of concern in the present study).

Fig. 7b depicts $Nu_x Re_x^{-1/2}$ variation with Ri_x for $Pr = 1$ and different values of B. The pure forced and pure natural convection asymptotes are also shown for comparison. Two dashed lines are drawn to distinguish between the pure forced convection regime (region I), the mixed convection regime (region II) and the pure natural convection regime (region III). It is noted that

the mixed convection regime extends over $0.1 < Ri_x < 40$ with the lower limit depending upon the value of B which, generally, increases with B. Here, similarity method solutions are not applicable and local similarity and/or local non-similarity methods may be used. It is also noted that the heat transfer results in the mixed convection region are affected by B for $B > 10^{-4}$. Besides, for $B < 10^{-4}$, $Nu_x Re_x^{-1/2}$ approaches asymptotically the pure forced convection value of 0.4438, as reported by Jacobi (1993), before it starts to increase with Ri_x due to buoyancy effect. This suggests that a self-similar forced-convection dominated region exits, the extent of this region depends upon the value of B. The self-similar dimensionless temperature profiles shown earlier in Fig. 6c indicated that such a region would exist even for a value of B as high as 10^{-2}.

The curves for different values of B shown in Fig. 7b correspond generally to low values of Re_x at which the stream-wise diffusion is important and hence the hydrothermal characteristics are non-similar. Since $Re_x = Ri_x/B$, therefore as Ri_x increases for a given value of B, Re_x increases and the characteristics become self-similar as the stream-wise diffusion vanishes. Accordingly, all curves meet and collapse onto a single line with increasing Ri_x as shown. This single line approaches gradually, at large Ri_x, the pure natural-convection asymptotic value. The latter value can be found in, for example, Kays and Crawford (1993).

Fig. 8a shows the variation of $Nu_x Re_x^{-1/2}$ versus Ri_x for $B = 10^{-2}$ with the Prandtl number as a parameter. The circles on the solid lines mark both $Ri_{x,c1}$ and $Ri_{x,c2}$ and the dashed lines connecting these circles, therefore, distinguish between the forced convection regime to the left (region I), the mixed convection regime at the middle (region II) and the natural convection regime to the right (region III). In general, $Ri_{x,c1}$ and $Ri_{x,c2}$ increase with Pr. The exception is for $Ri_{x,c1}$ for $Pr = 0.1$ where $Ri_{x,c1}$ decreases a little and then increases with increasing Pr. It is evident that $Nu_x Re_x^{-1/2}$ increases with Pr for a given Ri_x, as expected. Also, the heat transfer results become independent of Pr at low Ri_x ($Ri_x < 10^{-3}$ for $B = 10^{-2}$ and $Pr \leqslant 10$) and would have a power law variation with Ri_x. This is since the problem becomes diffusion dominated and, hence, independent of Pr.

Fig. 8b presents the corresponding local skin-friction coefficient variation over the surface in terms of $C_{f,x} Re_x^{1/2}$ versus Ri_x. Similar remarks may be made to those discussed in Fig. 3b. Besides, it is interesting to note that the friction coefficient becomes independent of Pr for $Ri_x < 0.2$ since forced convection becomes dominant and, hence, the hydrodynamics become independent of the heat transfer. It is also noted that the locations of the vanishing shear stress at the plate surface ($C_{f,x} = 0$) move downstream as Pr increases. These locations are: $Ri_x = 0.76$, 0.80, 0.97, 1.28 and 1.88 for $Pr = 0.1$, 0.3, 1, 3 and 10, respectively, and $B = 10^{-2}$.

Finally, maps for delineating the forced, mixed and natural convection regimes are developed. These maps are presented as a function of Reynolds number and Grashof number for $B = 10^{-2}$ and for $Pr = 0.1$, 1, 3 and 10 in Fig. 9a–d, respectively. The mixed convection regime is bound by two boundaries shown in the figures which are determined from the critical values of Richardson number. The two boundaries are: an upper forced-convection boundary which separates the forced convection from the mixed convection regimes, and a lower natural-convection boundary which separates the mixed convection from the natural convection regimes. The critical values of Richardson number are determined according to the 5% criterion discussed earlier.

Equations that define the dividing boundaries are also shown on Fig. 9a–d. These equations are power law equations with coefficients calculated from the critical values of Richardson number ($Ri_{x,c1}$ and $Ri_{x,c2}$) according to

$$Re_x = Ri_{x,c}^{-1/2} Gr_x^{1/2} \tag{12}$$

Ranges of Richardson number for the various convection regimes are summarized in Table 1; values of $Ri_{x,c1}$

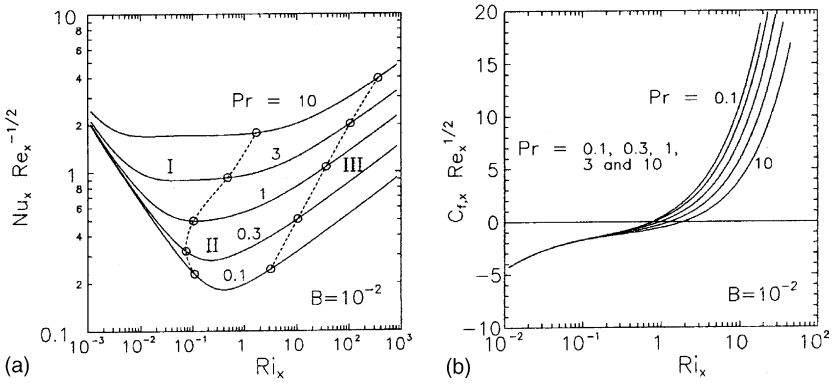

Fig. 8. Nusselt number and skin-friction coefficient variations with Richardson number for $B = 10^{-2}$ and different Pr; (a) Nusselt number, and (b) skin-friction coefficient.

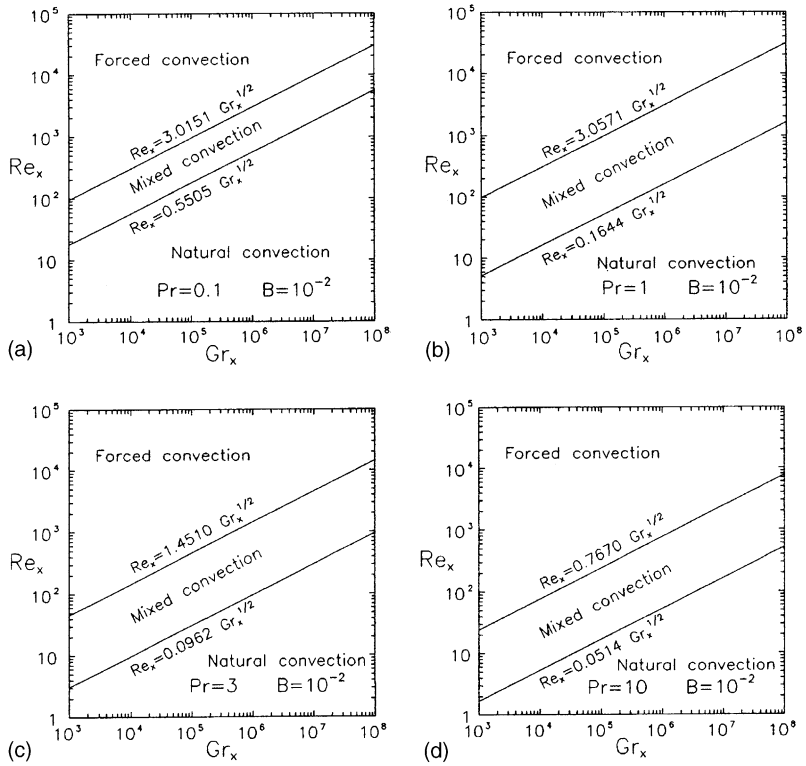

Fig. 9. Regimes of forced, mixed and natural convection for $B = 10^{-2}$; (a) $Pr = 0.1$, (b) $Pr = 1$, (c) $Pr = 3$, and (d) $Pr = 10$.

Table 1
Range of Richardson number (Ri_x) for the various convection regimes showing the effect of Prandtl number (Pr) and buoyancy force parameter (B)[a]

Pr	B	Forced convection	Mixed convection	Natural convection
0.1	10^{-4}	$Ri_x < 0.006$	$0.006 \leqslant Ri_x \leqslant 3.3$	$Ri_x > 3.3$
1	10^{-4}	$Ri_x < 0.136$	$0.136 \leqslant Ri_x \leqslant 37$	$Ri_x > 37$
3	10^{-4}	$Ri_x < 0.525$	$0.525 \leqslant Ri_x \leqslant 108$	$Ri_x > 108$
10	10^{-4}	$Ri_x < 1.73$	$1.73 \leqslant Ri_x \leqslant 374$	$Ri_x > 374$
0.1	10^{-3}	$Ri_x < 0.026$	$0.026 \leqslant Ri_x \leqslant 3.3$	$Ri_x > 3.3$
1	10^{-3}	$Ri_x < 0.115$	$0.115 \leqslant Ri_x \leqslant 37$	$Ri_x > 37$
3	10^{-3}	$Ri_x < 0.511$	$0.511 \leqslant Ri_x \leqslant 108$	$Ri_x > 108$
10	10^{-3}	$Ri_x < 1.70$	$1.70 \leqslant Ri_x \leqslant 374$	$Ri_x > 374$
0.1	10^{-2}	$Ri_x < 0.110$	$0.110 \leqslant Ri_x \leqslant 3.3$	$Ri_x > 3.3$
1	10^{-2}	$Ri_x < 0.107$	$0.107 \leqslant Ri_x \leqslant 37$	$Ri_x > 37$
3	10^{-2}	$Ri_x < 0.475$	$0.475 \leqslant Ri_x \leqslant 108$	$Ri_x > 108$
10	10^{-2}	$Ri_x < 1.70$	$1.70 \leqslant Ri_x \leqslant 378$	$Ri_x > 378$
0.1	10^{-1}	$Ri_x < 0.468$	$0.468 \leqslant Ri_x \leqslant 3.3$	$Ri_x > 3.3$
1	10^{-1}	$Ri_x < 0.240$	$0.240 \leqslant Ri_x \leqslant 38$	$Ri_x > 38$
3	10^{-1}	$Ri_x < 0.376$	$0.376 \leqslant Ri_x \leqslant 111$	$Ri_x > 111$
10	10^{-1}	$Ri_x < 1.61$	$1.61 \leqslant Ri_x \leqslant 378$	$Ri_x > 378$
0.1	1	$Ri_x < 2.08$	$2.08 \leqslant Ri_x \leqslant$ –[b]	$Ri_x >$ –[b]
1	1	$Ri_x < 0.85$	$0.85 \leqslant Ri_x \leqslant 40$	$Ri_x > 40$
3	1	$Ri_x < 0.70$	$0.70 \leqslant Ri_x \leqslant 117$	$Ri_x > 117$
10	1	$Ri_x < 1.29$	$1.29 \leqslant Ri_x \leqslant 381$	$Ri_x > 381$

[a] The two critical Richardson numbers, $Ri_{x,c1}$ and $Ri_{x,c2}$, are the lower and upper limits in the mixed convection region.
[b] $Ri_{x,c2}$ could not be obtained since the 5% criterion overshot the mixed convection results throughout the whole region.

and $Ri_{x,c2}$ can, in turn, be substituted in Eq. (12) to obtain the corresponding equations for the dividing lines.

The convection map for $Pr = 0.1$, shown in Fig. 9a, is characterized by a relatively narrow mixed convection regime. In general, for a given Gr_x, the Re_x range that

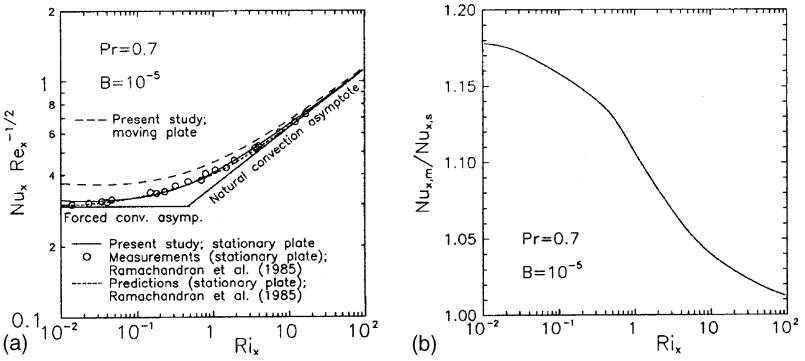

Fig. 10. Nusselt number variation with Richardson number for $Pr = 0.7$ and $B = 10^{-5}$ showing comparison between moving and stationary plates; (a) Nusselt number, and (b) Nusselt number ratio.

identifies the mixed convection regime decreases with increasing Pr. Also, the change from the forced convection regime to the natural convection regime, for a given Re_x, occurs over a range of Gr_x that increases with Pr. Note that the width or height of the mixed convection band, as it looks on the figure, is not indicative of the actual range of values because of the logarithmic scales.

The convection regime maps are useful in the sense that when $Ri_x < Ri_{x,c1}$, natural convection effects can be ignored; if $Ri_x > Ri_{x,c2}$, forced convection effects can be ignored. The results in Fig. 9a–d along with other results for different values of B are summarized in Table 1. To the author's best knowledge, convection regime maps of the moving plate problem (backward boundary layer) have not been previously developed.

3.4. Comparison between the moving and stationary plates

It is interesting to compare the results for the continuously moving plate in an otherwise a stationary fluid with those for the moving fluid over a stationary plate. For the latter problem, the boundary conditions correspond to $u = 0$ at $y = 0$ and $u = u_\infty$ as $y \to \infty$ in which case the situation is simply transformed to a Blasius-type problem. Fig. 10a presents the local Nusselt number variation along the plate for the two respective cases calculated for $Pr = 0.7$ and $B = 10^{-5}$. The present results for the case of the moving fluid over a stationary plate are also compared with the experimental measurements and predictions of Ramachandran et al. (1985) showing excellent agreement. The forced and natural convection asymptotes, see for example Kays and Crawford (1993), are shown for comparison. These asymptotes illustrate the region where mixed convection results deviate from the pure forced convection and pure natural convection values. It is noted that u_∞ is the free-stream velocity and that Re_x and Ri_x for the case of the stationary plate are based on u_∞. As can be seen from Fig. 10a, Nu_x and, hence, the heat transfer rates are higher for the moving plate case for any given value of Ri_x. The results of the two cases approach the same natural convection asymptote at large Ri_x.

Fig. 10b shows a comparison of the two cases in terms of $Nu_{x,m}/Nu_{x,s}$ variation with Ri_x; the subscripts m and s denote the moving and stationary plates, respectively. This local Nusselt number ratio is greater than one and decreases with increasing Ri_x. At $Ri_x = 10^{-2}$, i.e. in the forced-convection dominated region, the ratio is about 1.18 and compares very well with the value of 1.1846 as would have been calculated by Tsou et al. (1967) and Jacobi (1993) under pure forced convection conditions. On the other hand, at $Ri_x = 10^2$, i.e. in the natural-convection dominated region, the ratio is about 1.01 and approaches one at larger Ri_x. This is expected since the differences between the two cases; namely, Blasius- and Sakiadis-type problems, diminish as the buoyancy forces dominate over the inertia forces.

4. Conclusions

The heat transfer and friction characteristics along a continuously moving vertical sheet of extruded material in an otherwise quiescent fluid were studied close to and far downstream from the extrusion slot. The numerical model, based on a finite volume procedure, was validated against published results available for special situations with excellent agreement. Regimes of forced, mixed and natural convection have been delineated, in buoyancy assisting flows, as a function of Reynolds and Grashof numbers for different values of Prandtl number and buoyancy force parameter. Under the conditions and range of parameters investigated in the present study the following remarks are made.

(1) At low Ri_x, the heat transfer rates due to different convection modes are all equal. This is attributed to the fact that diffusion dominates over both inertia and buoyancy in the region close to the extrusion

slot. Little further downstream, inertia forces start to show an effect as the stream-wise diffusion diminishes. Therefore, heat transfer enhancement over that of pure natural convection takes place. Further downstream, the buoyancy forces start to have an effect and the mixed convection results deviate from the forced convection results. Heat transfer enhancement due to buoyancy forces continues with distance downstream and, as the buoyancy forces dominate over the inertia forces, the heat transfer rate due to pure natural convection, once again, equals that of the mixed convection at large Ri_x.

(2) The heat transfer rate drops sharply with distance in the non-similar forced-convection dominated region. The drop continues downstream but at a slower rate as the thermal boundary layer thickens.
(3) Critical values of Gr_x were determined for different Pr that distinguish the non-similar pure natural-convection region from the self-similar region. It was found that $Gr_{x,c}$ decreases as Pr increases.
(4) The heat transfer results in the mixed convection region are affected by the buoyancy force parameter (B) for $B > 10^{-4}$.
(5) The existence and extent of a self-similar forced-convection dominated region depend upon the value of B. This region is diminished for $B > 10^{-2}$.
(6) At low Ri_x, the heat transfer results become independent of Prandtl number and the convection mode.
(7) The vanishing shear stress at the plate surface is located at $0.76 \leqslant Ri_x \leqslant 1.88$ for $0.1 \leqslant Pr \leqslant 10$ and $B = 10^{-2}$. The friction coefficient becomes independent of Pr for $Ri_x < 0.2$.
(8) In general, the extent of the forced-convection dominated regime increases with Pr and, hence, the location of the mixed convection regime is moved downstream.
(9) For a given Re_x, the transition from the forced convection regime to the natural convection regime occurs over a range of Gr_x that increases with Pr.
(10) Comparisons of mixed convection results between the moving and stationary plates show that the heat transfer rate for the moving plate is higher than that for the stationary plate for given Pr, B and Ri_x. The difference in results between the two cases decreases as Ri_x increases and diminishes as the buoyancy forces dominate over the inertia forces.

As a final note of caution, laminar flow is assumed to be valid for the entire mixed convection regime that is presented in the study. This laminar assumption limits the applicability to situations with relatively low velocity, i.e. $Re_x < 5 \times 10^5$ and/or $Ra_x = Gr_x Pr < 10^9$. Turbulent flow must be considered in high velocity situations. Also, it is emphasized that since the results were obtained from numerical solution of the laminar governing equations, therefore, they do not account for the outside physical effects that may cause instability and transition to turbulence.

References

Ali, M.E., 1994. Heat transfer characteristics of a continuous stretching surface. Wärme- und Stoffübertragung 29, 227–234.

Ali, M.E., Al-Yousef, F., 1998. Laminar mixed convection from a continuously moving vertical surface with suction or injection. Heat and Mass Transfer 33 (4), 301–306.

Al-Sanea, S.A., Ali, M.E., 2000. The effect of extrusion slit on the flow and heat-transfer characteristics from a continuously moving material with suction or injection. International Journal of Heat and Fluid Flow 21, 84–91.

Al-Sanea, S.A., Pun, W.M., Spalding, D.B., 1980. Computation of two-dimensional elliptic flows, including heat transfer. In: Morgan, K., Taylor, C., Brebbia, C.A. (Eds.), Computer Methods in Fluids. Pentech Press, London, pp. 217–256.

Altan, T., Oh, S., Gegel, H., 1979. Metal Forming Fundamentals and Applications. American Society of Metals, Metals Park, OH.

Chen, C.-H., 1998. Laminar mixed convection adjacent to vertical, continuously stretching sheets. Heat and Mass Transfer 33, 471–476.

Chen, C.-H., 2000. Mixed convection cooling of a heated, continuously stretching surface. Heat and Mass Transfer 36, 79–86.

Chen, T.S., Armaly, B.F., 1987. Mixed convection in external flow. In: Kakac, S., Shah, R.K., Aung, W. (Eds.), Handbook of Single-Phase Convective Heat Transfer. Wiley, New York, pp. 14.1–14.35 (Chapter 14).

Chen, T.S., Strobel, F.A., 1980. Buoyancy effects on heat and mass transfer in boundary layer on a continuous, moving horizontal plate. Numerical Heat Transfer 3, 115–130.

Chida, K., Katto, Y., 1976. Conjugate heat transfer of continuously moving surfaces. International Journal of Heat and Mass Transfer 19, 461–470.

Fan, J.R., Shi, J.M., Xu, X.Z., 1997. Similarity solution of mixed convection over a horizontal moving plate. Heat and Mass Transfer 32, 199–206.

Fan, J., Shi, J., Xu, X., 1999. Similarity solution of free convective boundary-layer behavior at a stretching surface. Heat and Mass Transfer 35, 191–196.

Fisher, E.G., 1976. Extrusion of Plastics. Wiley, New York.

Grubka, L.G., Bobba, K.M., 1985. Heat transfer characteristics of a continuous stretching surface with variable temperature. ASME Journal of Heat Transfer 107, 248–250.

Jacobi, A.M., 1993. A scale analysis approach to the correlation of continuous moving sheet (backward boundary layer) forced convective heat transfer. ASME Journal of Heat Transfer 115, 1058–1061.

Jeng, D.R., Chang, T.C.A., De Witt, K.J., 1986. Momentum and heat transfer on a continuous moving surface. ASME Journal of Heat Transfer 108, 532–539.

Kang, B.H., Jaluria, Y., 1994. Heat transfer from continuously moving material in channel flow for thermal processing. Journal of Thermophysics and Heat Transfer 8 (3), 546–554.

Karwe, M.V., Jaluria, Y., 1988. Fluid flow and mixed convection transport from a moving plate in rolling and extrusion processes. ASME Journal of Heat Transfer 110, 655–661.

Karwe, M.V., Jaluria, Y., 1991. Numerical simulation of thermal transport associated with a continuously moving flat sheet in materials processing. ASME Journal of Heat Transfer 113, 612–619.

Kays, W.M., Crawford, M.E., 1993. Convective Heat and Mass Transfer, third ed. McGraw-Hill, New York.

Moutsoglou, A., Chen, T.S., 1980. Buoyancy effects in boundary layers on inclined, continuous, moving sheets. ASME Journal of Heat Transfer 102, 371–373.

Patankar, S.V., Spalding, D.B., 1972. A calculation procedure for heat, mass and momentum transfer in three-dimensional parabolic flows. International Journal of Heat and Mass Transfer 15, 1787–1806.

Pun, W.M., Spalding, D.B., 1977. A general computer program for two-dimensional elliptic flows. Report no. HTS/76/2, Department of Mechanical Engineering, Imperial College, London.

Ramachandran, N., Armaly, B.F., Chen, T.S., 1985. Measurements and predictions of laminar mixed convection flow adjacent to a vertical surface. ASME Journal of Heat Transfer 107, 636–641.

Sakiadis, B.C., 1961a. Boundary-layer behavior on continuous solid surfaces: I. Boundary-layer equations for two-dimensional and axisymmetric flow. AIChE Journal 7, 26–28.

Sakiadis, B.C., 1961b. Boundary-layer behavior on continuous solid surfaces: II. The boundary layer on a continuous flat surface. AIChE Journal 7, 221–225.

Schlichting, H., 1979. Boundary-Layer Theory, seventh ed. McGraw-Hill, New York.

Soundalgekar, V.M., Ramana Murty, T.V., 1980. Heat transfer in flow past a continuous moving plate with variable temperature. Wärme- und Stoffübertragung 14, 91–93.

Strobel, F.A., Chen, T.S., 1980. Buoyancy effects on heat and mass transfer in boundary layers adjacent to inclined, continuous, moving sheets. Numerical Heat Transfer 3, 461–481.

Tadmor, Z., Klein, I., 1970. Engineering Principles of Plasticating Extrusion, Polymer Science and Engineering Series. Van Nostrand Reinhold, New York.

Tsou, F.K., Sparrow, E.M., Goldstein, R.J., 1967. Flow and heat transfer in the boundary layer on a continuous moving surface. International Journal of Heat and Mass Transfer 10, 219–235.

Viskanta, R., Bergman, T.L., 1998. Heat transfer in materials processing. In: Rohsenow, W.M., Hartnett, J.P., Cho, Y.I. (Eds.), Handbook of Heat Transfer, third ed. McGraw-Hill, New York, pp. 18.1–18.74 (Chapter 18).